Article

Cell

Developmental Acquisition of Regulomes Underlies Innate Lymphoid Cell Functionality

Graphical Abstract

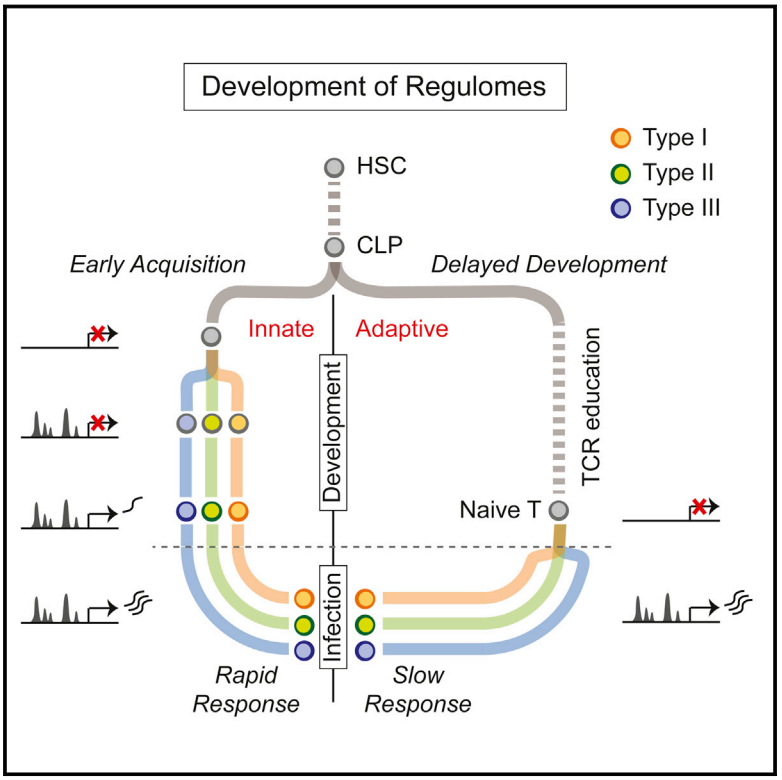

Authors

Han-Yu Shih, Giuseppe Sciumè, Yohei Mikami, ..., Fred P. Davis, Yuka Kanno, John J. O'Shea

Correspondence

han-yu.shih@nih.gov (H.-Y.S.), john.oshea@nih.gov (J.J.O.)

In Brief

Innate lymphoid cells and adaptive T helper cells become specialized cytokine-producing cells by distinct, but converging, routes.

Highlights

- Prototypical ILC subsets show distinctive regulomes
- Regulatory elements of ILC effector genes are poised prior to activation
- Regulomes of ILC subsets diverge early at precursor stages
- Regulomes of innate and adaptive cells converge upon infection

Accession Numbers

GSE77695

Shih et al., 2016, Cell *165*, 1120–1133
May 19, 2016 Published by Elsevier Inc.
http://dx.doi.org/10.1016/j.cell.2016.04.029

Cell

Article

Developmental Acquisition of Regulomes Underlies Innate Lymphoid Cell Functionality

Han-Yu Shih,[1,5,*] Giuseppe Sciumè,[1,5] Yohei Mikami,[1,5] Liying Guo,[2] Hong-Wei Sun,[3] Stephen R. Brooks,[3] Joseph F. Urban, Jr.,[4] Fred P. Davis,[1] Yuka Kanno,[1] and John J. O'Shea[1,*]

[1]Lymphocyte Cell Biology Section, Molecular Immunology and Inflammation Branch, National Institute of Arthritis and Musculoskeletal and Skin Diseases

[2]Laboratory of Immunology, National Institute of Allergy and Infectious Diseases

[3]Biodata Mining and Discovery Section, National Institute of Arthritis and Musculoskeletal and Skin Diseases

National Institutes of Health, Bethesda, MD 20892, USA

[4]Diet, Genomics, and Immunology Laboratory, Beltsville Human Nutrition Research Center, Agricultural Research Service, U.S. Department of Agriculture, Beltsville, MD 20705, USA

[5]Co-first author

*Correspondence: han-yu.shih@nih.gov (H.-Y.S.), john.oshea@nih.gov (J.J.O.)

http://dx.doi.org/10.1016/j.cell.2016.04.029

SUMMARY

Innate lymphoid cells (ILCs) play key roles in host defense, barrier integrity, and homeostasis and mirror adaptive CD4$^+$ T helper (Th) cell subtypes in both usage of effector molecules and transcription factors. To better understand the relationship between ILC subsets and their Th cell counterparts, we measured genome-wide chromatin accessibility. We find that chromatin in proximity to effector genes is selectively accessible in ILCs prior to high-level transcription upon activation. Accessibility of these regions is acquired in a stepwise manner during development and changes little after in vitro or in vivo activation. Conversely, dramatic chromatin remodeling occurs in naive CD4$^+$ T cells during Th cell differentiation using a type-2-infection model. This alteration results in a substantial convergence of Th2 cells toward ILC2 regulomes. Our data indicate extensive sharing of regulatory circuitry across the innate and adaptive compartments of the immune system, in spite of their divergent developing pathways.

INTRODUCTION

The immune system orchestrates host defense through complex effector networks mediated by an array of lymphocytes, including conventional T, B, and natural killer (NK) cells, along with an array of recently recognized innate lymphoid cells (ILCs) (Artis and Spits, 2015; Diefenbach et al., 2014; Eberl et al., 2015; Sonnenberg and Artis, 2015). Unlike T and B cells, which mediate adaptive immunity against pathogenic microbes in an antigen-specific manner, ILCs respond to invaders promptly in the absence of somatically rearranged antigen receptors. Three classes of ILCs are presently recognized and categorized based on their selective cytokine-production profiles, mirroring previously identified CD4$^+$ Th cell subsets (Spits et al., 2013; Verykokakis et al., 2014). Group 1 ILCs include conventional NK cells, the first identified ILC subset, along with ILC1s, which lack the cytotoxicity capability of NK cells. Both of these cells selectively produce interferon (IFN)-γ, the key cytokine that defines T helper (Th) 1 cells. Group 2 ILCs (encompassing ILC2) preferentially produce cytokines such as interleukin (IL)-5, IL-13, and IL-9, originally defined as Th2 cytokines. Finally, group 3 ILCs are a heterogeneous subset that comprises natural cytotoxicity receptor (NCR)-positive ILC3s and CD4-positive ILC3s (also known as lymphoid tissue inducer-like [LTi] cells) that produce IL-17 and/or IL-22, the namesake cytokines of Th17 and/or Th22 cells.

Several important issues remain unresolved, including the regulatory mechanisms underlying ILC development, diversification, and terminal differentiation and how these mechanisms compare to those of Th cell subsets. Like T and B lymphocytes, ILCs are derived from common lymphoid progenitors (CLPs), and are further specified by an array of transcription factors (TFs) (De Obaldia and Bhandoola, 2015; Kang and Malhotra, 2015; Klose and Diefenbach, 2014). The transcriptional regulator inhibitor of DNA binding 2, Id2, for instance, counteracts the effects of E proteins to limit the development of T and B lymphocytes. Other TFs, such as Nfil3, Plzf, Tox, Tcf7, and Runx3, are also involved in the lineage divergence during ILC development (Serafini et al., 2015). However, consistent with their selective cytokine production, ILCs also use the same lineage-determining transcription factors (LDTFs) that drive cognate T cell-lineage specification (Shih et al., 2014; Spits et al., 2013). For instance, T-box transcription factors, including Eomesodermin and T-bet (encoded by *Eomes* and *Tbx21* genes, respectively), are involved in the specification of all IFN-γ producers, whereas Th2 and Th17 master regulators GATA-binding protein 3 (GATA-3) and retinoic acid receptor-related orphan receptor γt (RORγt) are essential for the development of group 2 and 3 ILCs, respectively. However, the extent to which the ontogeny of ILCs truly parallels Th cell specification, especially at the genomic level, remains poorly understood.

Beyond the assessment of selective cytokine production and enumeration of LDTFs, the relationships between lineages can

also be probed with genomic tools. Both microarray and RNA sequencing have been extensively used to delineate cell-type-specific transcriptomes (Kim and Lanier, 2013; Shay and Kang, 2013). Recently reported ILC transcriptomes suggest that the tissue microenvironment also has a substantial impact on gene expression profiles beyond lineage per se (Robinette et al., 2015). Thus, defining cell identity by transcriptome requires careful consideration of the local "environmental" factors and tissue residency.

Another strategy of determining cell-fate and lineage relationships is to analyze global epigenetic information, which, in contrast to gene expression, can be more stable and propagate information over time during development and differentiation (Bornstein et al., 2014; Lara-Astiaso et al., 2014). Epigenetic codes, including DNA methylation, histone modifications, and chromatin accessibility, together construct unique chromatin landscapes at non-coding regulatory elements (REs), which contribute to gene expression by permitting or restricting access of transcriptional machinery to key loci.

It is now appreciated that distinct lineages exhibit thousands of highly distinctive genomic "switches," which act in concert to govern tissue-specific and temporal control of gene expression. Among epigenomic elements, enhancers are intriguing due to their ability to control gene expression at a distance and contribute to lineage specificity (Heinz et al., 2015). Genome-wide enhancer distribution has been mapped in various lineages based on the characteristics of chromatin accessibility, histone modifications, and TF binding. Accumulating data reveal that the basal epigenomes (prior to cell activation) encode cell-fate information and are progressively specified in response to developmental cues and environmental stimuli (Lara-Astiaso et al., 2014; Stergachis et al., 2014; Vahedi et al., 2012). Recent studies on macrophages highlight the environmental impact on tissue-specific chromatin states (Gosselin et al., 2014; Lavin et al., 2014). However, the contribution of development versus environment to the fate of ILC identity has not been systematically characterized at the genomic level.

In this study, we set out to answer a number of questions related to ILC ontogeny and regulation and their relationships with cognate adaptive immune cells. Using genomic tools, we comprehensively identified REs that comprise the lineage-specific regulome in conjunction with measuring transcriptomes of prototypical ILCs and their progenitors. Our genome-wide analysis revealed that each ILC lineage possesses unique open chromatin landscapes and conforms to the general view of ILC1, ILC2, and ILC3 as distinct lineages. These features were relatively static after ILC activation, despite dynamic changes in gene expression, revealing the poised status of ILCs prior to stimulation. The presence of lineage-specific REs in ILC precursors indicates that ILC functionality is pre-determined as the cells diverge into definite lineages. In contrast, naive T cells exhibit markedly different chromatin landscapes that change dramatically after activation and final differentiation. Nonetheless, their regulomes converge with those of ILCs. The substantial overlap of REs between Th cells and ILCs is striking, given their distinct routes of development. Together, our data provide mechanistic underpinnings for ILC-lineage commitment, acquisition of poised functionalities, as well as the relationships between innate and adaptive compartments.

RESULTS

The Chromatin Landscapes of Innate Lymphocyte Lineages Reflect Their Distinct Functionalities

ILCs have been categorized into three major groups based on selective cytokine production that parallel Th cell subsets (Spits et al., 2013). To better understand the regulatory logic of ILCs, we globally identified REs in the major types by an assay for transposase-accessible chromatin using sequencing (ATAC-seq). This method requires few cells, enabling us to characterize the regulomes of cells directly isolated ex vivo (Buenrostro et al., 2013). In parallel, we also assessed transcriptomes by RNA-seq. We first analyzed five prototypical ILC subsets, including conventional NK cells from spleen and ILC1s from liver (group 1); ILC2s from small intestine lamina propria (siLP; group 2); and $CD4^+$ (LTi-like ILC3s) and NCR^+ ILC3s, both from siLP (group 3). These subsets were chosen based on the possibility of distinguishing their identity using accepted surface markers (Figures 1A and S1A) and were confirmed by the expression of their LDTFs (Figure S1B).

We first examined chromatin landscapes of ILC-signature cytokines that were differentially expressed in ILCs (Figures 1B and S1C–S1E). We found that the lineage-specific chromatin landscapes correlated with the recognized functionality of each subset. The distinct patterns of accessibility encompassed not only promoters but also intragenic and intergenic regions, extending as far as several kilobases away (highlighted in blue and red, respectively). These accessible regions included REs previously characterized in the *Ifng*, *Il4/5/13*, *Il17*, and *Il22* loci (Figures 1B and S1D, red triangles; Balasubramani et al., 2010; Wilson et al., 2009), as well as multiple lineage-specific REs not previously identified. Most of these REs appear to be putative enhancers, as they co-localized with p300 and T-bet binding in NK cells, the latter being a critical TF known to regulate *Ifng* (Figure 1B). Notably, three *Ifng*-associated REs were specific for NK cells and absent in ILC1s (Figure 1B, red arrows), suggesting that the same locus might be differentially regulated in distinct IFN-γ-producing cells. On the other hand, an ILC2-specific RE 40 kb downstream of the *Ifng* gene showed GATA-3 binding in ILC2s (Zhong et al., 2016), suggesting the possibility of regulation by LDTFs, which antagonize alternative cell fates. We also observed that distinct REs at LDTF loci were accessible even in the absence of their expression, which may indicate opportunities for functional plasticity (Figures 1C, S1F, and S1G). For example, a portion of *Rorc* and *Il17* REs was accessible in ILC2s; this phenomenon may explain previous observations of IL-17 production in these cells (Huang et al., 2015). In addition, type 3 ILCs have been reported to express T-bet and produce low levels of IFN-γ (Bernink et al., 2013; Klose et al., 2013; Rankin et al., 2013; Sciumé et al., 2012); accordingly, our data revealed that a portion of IFN-γ REs, including the promoter and distal T-bet binding sites, was accessible in NCR^+ ILC3s but not in $CD4^+$ ILC3s. Taken together, high-resolution profiling of chromatin landscapes by ATAC-seq identified lineage-specific REs near genes that specify ILC functions.

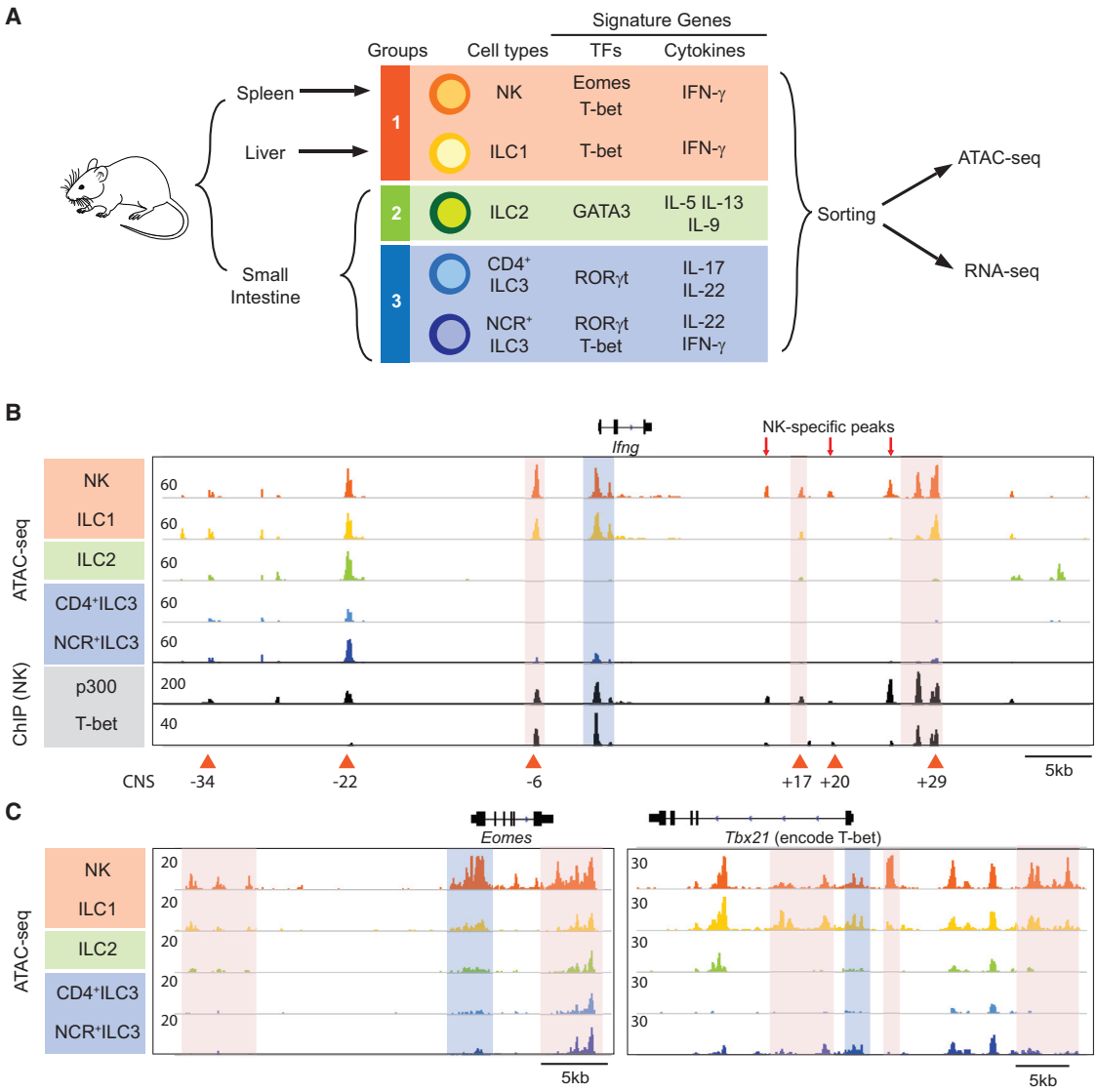

Figure 1. Identification of Regulatory Elements of Innate Lymphoid Cells

(A) Schematic illustration of experimental design. Five prototypical ILCs from various organs were isolated by flow cytometry for ATAC-seq and RNA-seq analysis. Listed in the table are ILC-signature genes. All experiments were done in duplicate.

(B and C) Representative examples of normalized ATAC-seq signal profiles in ILCs across type 1 signature genes including (B) *Ifng* and (C) *Eomes* and *Tbx21*. (B) p300 and T-bet ChIP-seq were acquired from NK cells.

Lineage-signature ATAC peaks at promoter and non-promoter regions are highlighted in blue and red, respectively. Red triangles denote known regulatory elements (Balasubramani et al., 2010; Wilson et al., 2009). Red arrows denote NK cell-specific REs.

See also Experimental Procedures and Figure S1.

Global Views of ILC Chromatin Landscapes Reveal Differential Regulomes

Next, we sought to obtain a global picture of ILC regulomes by analyzing accessible REs genome-wide. Among a total of 82,305 accessible REs merged from five prototypical ILCs, about a quarter were common to all subsets, whereas the majority (75%) of the regions were either unique to a single cell type or shared by a subset of ILCs (here termed variable regions) (Figures 2A and 2B). As expected, differential RE accessibility was correlated with selective gene expression in ILC subsets (Figure S2A). Analyzing the genomic distribution of ILC REs revealed that promoters (REs within ±1 kb of transcription start sites) were preferentially enriched among common REs (30%) but were depleted from variable REs (5%) (Figure 2C). This observation suggests that the divergence of ILC chromatin landscapes appears to be primarily shaped by distal REs.

For each lineage, we defined ATAC-accessible regions that are not ubiquitously accessible in all lineages as their "signature REs," which differ from "specific REs," which are exclusively accessible in only one lineage.

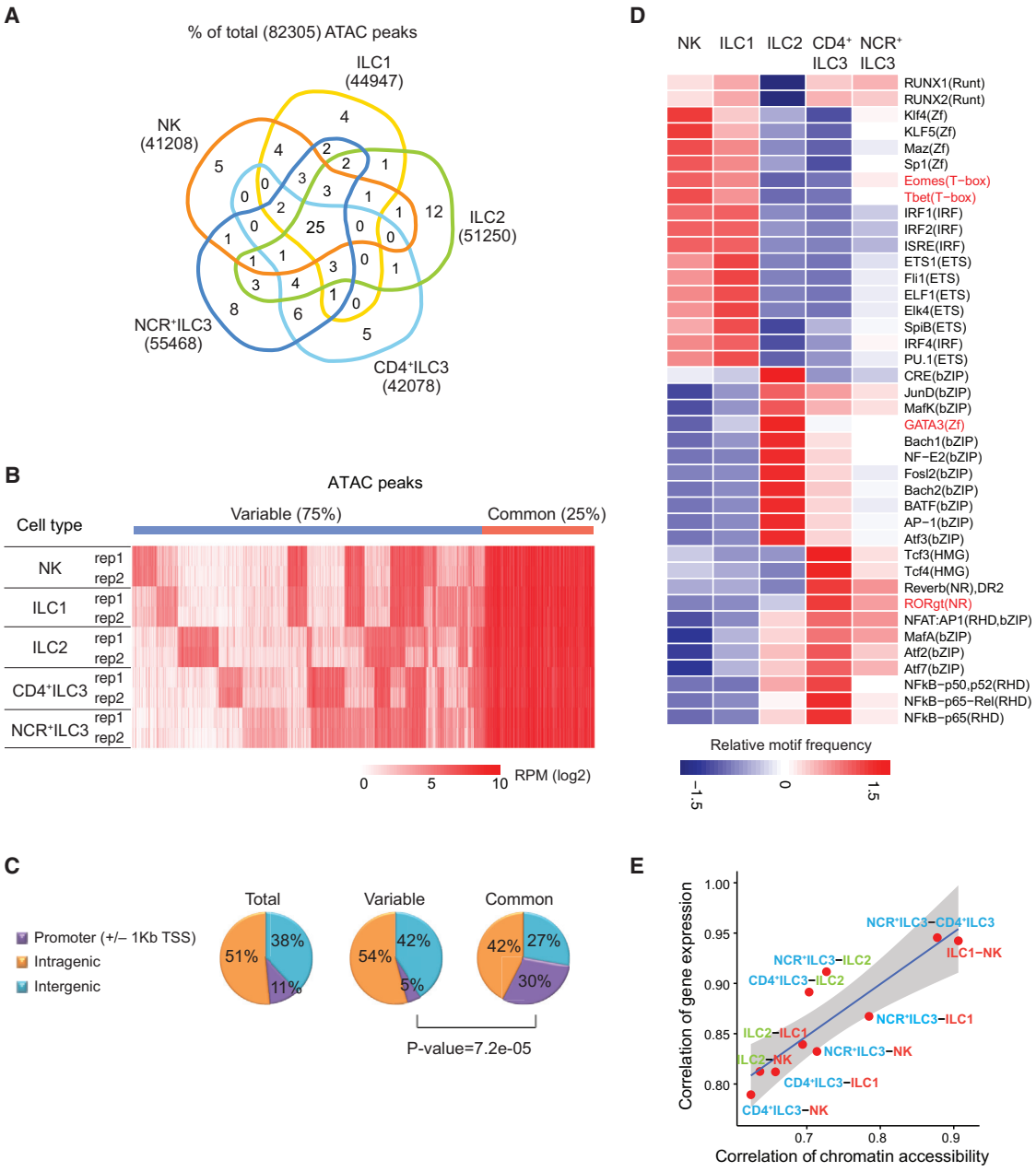

Figure 2. Genome-Wide Chromatin Landscapes Define Distinct ILC Subsets

(A and B) Comparison of global ATAC peaks in prototypical ILCs. (A) Venn diagram demonstrating percentages of ATAC peaks that are commonly or differentially present in ILCs. The total number of ATAC peaks in each ILC subset is indicated with the annotation. (B) Heatmap showing signal intensity (reads per million mapped reads by log2) of each ATAC peak.

(C) Pie charts illustrating the distribution of ATAC peaks across the genome (promoter, ±1 kb of transcription start sites [TSSs], and intragenic or intergenic regions). p value is determined by using Fisher's exact test.

(D) Heatmap showing relative enrichment of TF motifs among ILC-signature REs. LDTFs are highlighted in red.

(E) Scatterplot showing the relationships for Pearson correlations of transcriptomes and regulomes between pairs of ILC subsets. Log2-transformed tag counts averaged from replicates were used for Pearson correlation analysis with thresholds of 1 FPKM and 1 reads per million reads (RPM) for RNA-seq and ATAC-seq datasets, respectively. The blue line denotes the linear regression line derived from all data points in the plot. The gray area denotes 95% confidence limits of linear regression.

See also Experimental Procedures, Figure S2, and Table S1.

We next investigated potential TFs that could target ILC regulomes by searching for the enrichment of consensus TF motifs within signature REs. We found that target motifs for recognized LDTFs were differentially enriched among each ILC type, consistent with their known roles in driving ILC development (Figure 2D, highlighted in red). For instance, the T-box motif, which is shared by T-bet and Eomes, was prominent in group 1 ILC regulomes and depleted from those of ILC2s and ILC3s. Conversely, GATA-3 and RORγt motifs were enriched in group 2 and 3 ILCs, respectively. In addition to known LDTFs, we also identified other TFs potentially important for ILC specification that mirrored the enrichment pattern of known LDTFs (Figure 2D). For instance, the enrichment of Runx motifs in group 1 and 3 ILCs supports the very recent evidence of the essential role of Runx family members in their development (Ebihara et al., 2015). Because TFs belonging to a given family share the same motifs, we further filtered potential regulators based on their expression to identify both shared and unique regulatory networking modules for each ILC subset (Figure S2B). This analysis also recapitulated the fact that the TFs previously associated with NK cell development and/or function such as Ets and IRF family members (highlighted in the light red box) contribute to ILC regulation (Barton et al., 1998; Lohoff et al., 2000). In addition, NF-κB family members were identified in group 2 and 3 ILC regulatory networks (highlighted in the light blue box), correlated with the importance of IL-1β and IL-25/IL-33 functions in these subsets. Overall, these data point to distinctive regulomes that may reflect occupancy of key TFs contributing to ILC functionality and identity.

Having established the distinctive regulomes in ILCs, we next sought to determine how regulomes compared with transcriptomes in discerning ILC-lineage identity. Our data indicate that comparisons of accessible chromatin landscapes of different ILC groups reveal greater differences (Pearson correlation r = 0.62–0.78) than comparisons of expression profiles (Pearson correlation r = 0.79–0.91) (Figures 2E and S2C). Specifically, ILC transcriptomes revealed the highest similarity among group 1 cells (NK and ILC1) and group 3 cells ($CD4^+$ and NCR^+ ILC3) (Figure S2C, top). In addition, cells residing in the same tissue (intestinal ILC2 and group 3 ILC) also displayed high similarity. However, the comparison of regulomes provided a rather different view (Figure S2C, bottom). The differences among subsets in the same ILC group were more pronounced, and similarities of ILC2s and ILC3s were less obvious. In particular, comparing the regulomes of ILC2 and ILC3 subsets suggests that these cell types are more distinct than expected based on the similarities of their transcriptomes (Figure 2E).

ILC Regulomes Are Primed Prior to Activation

An important feature of ILCs is their ability to quickly respond to external cues and rapidly induce transcription and protein synthesis of effector genes to mediate host defense. Whether this process involves the rapid acquisition of new enhancers or utilization of pre-existing poised enhancers has not been determined. To understand the dynamics of enhancer landscapes and their impact on ILC activation, we stimulated NK, ILC2, and NCR^+ ILC3 cells with relevant cytokines for 4–6 hr and compared the changes in transcriptomes and regulomes with their resting state (Figures 3A and 3B). We observed more genes were downregulated than those that were upregulated in NK and NCR^+ ILC3 cells (>2-fold change, $p < 0.05$) upon stimulation, whereas similar numbers were up- and downregulated in ILC2 cells (Figure 3B, left). We also observed concordant changes in the number of ATAC-accessible sites that were accessible before and after stimulation (Figure 3B, right). This observation suggests that the dynamic changes of transcriptomes and regulomes might be well correlated. However, further global correlation analysis indicated that this was only partly true (Figures 3C and S3A). For instance, the transcriptomes of stimulated ILC2 and NCR^+ ILC3 cells were more similar to each other than those of unstimulated cells (Figure 3C). In contrast, assessment of their respective regulomes revealed that the distinctive REs were relatively stable, congruent with subset identity.

We next explored the dynamics of REs near cytokine loci that are rapidly induced upon stimulation (Figures 3D, S3B, and S3C). We found that even though transcript abundance increased dramatically, the chromatin landscapes of the *Ifng*, type 2 cytokine, and *Il22* loci changed little after activation. To further evaluate enhancer activity, we also investigated the dynamics of p300 binding and H3K27 acetylation levels in stimulated NK cells by chromatin immunoprecipitation sequencing (ChIP-seq) (Figure 3D). We found that most *Ifng* enhancers identified by ATAC-seq were pre-bound by p300 (12 of 13 sites) and were also H3K27 acetylated (7 of 13 sites) prior to activation. Upon stimulation, these sites exhibited enhanced p300 binding as well as increased H3K27 acetylation, whereas ATAC signals remained unchanged. The observed dynamic enhancer activity was consistent with enhanced cytokine production from the locus. This suggests that chromatin landscapes of stimulation-responsive elements are pre-determined before the cell is activated.

ILC Enhancer Landscapes Diverge Early in Development

Our finding that the enhancer landscapes of terminally differentiated ILCs are poised prior to cytokine stimulation raises the question of when these lineage-signature landmarks were initially established during development. To answer this, we profiled regulomes of developing ILCs, including immature NK (iNK), NK precursor (NKp), and ILC2 precursor (ILC2p) cells from bone marrow, and compared them with hematopoietic stem cells (HSCs), multipotent progenitor cells (MPPs), and common lymphoid progenitor cells (CLPs) (Figures 4A and S4A). The designation of NKp refers to lin^-CD122^{hi} cells enriched for cells committed to the NK fate (Chiossone et al., 2009; Constantinides et al., 2014; Fathman et al., 2011; Hoyler et al., 2012; Rosmaraki et al., 2001). Comparison of these cells revealed stepwise loss of HSC-signature REs and acquisition of ILC-signature REs during ILC development (Figures 4B and S4B). The loss of ~50% of the HSC-signature REs had already occurred in MPPs, with a further ~10% loss in CLPs and 20% loss in ILC precursors (NKp and ILC2p). Conversely, only 25%–30% of ILC-signature features were present in early progenitors (HSCs, MPPs, and CLPs), whereas another ~30% of these features were acquired as CLPs developed to NKp or ILC2p cells (Figure 4B). Of note, the later step involved minimum loss of HSC-signature REs. In aggregate, these data indicate that the regulatory landscapes of ILC precursors are at states that adopt ILC subset-signature chromatin landscapes while retaining progenitor features.

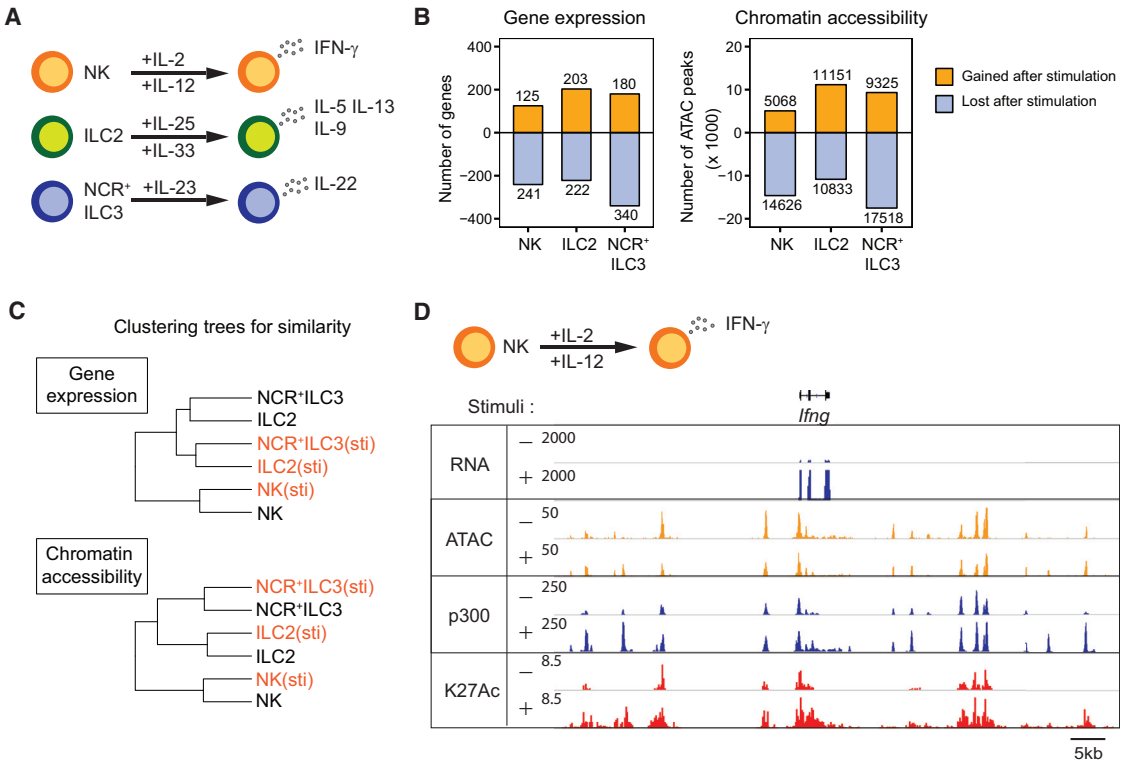

Figure 3. Cytokine Loci Are Primed Prior to Activation

(A) Experimental designs for ILC stimulation. NK cells were treated with IL-2 (1,000 U/ml) and IL-12 (10 ng/ml) for 6 hr; ILC2 cells were treated with IL-25 (50 ng/ml) and IL-33 (50 ng/ml) for 4 hr; and NCR$^+$ ILC3 cells were treated with IL-23 (50 ng/ml) for 4 hr.

(B) Changes in gene expression or chromatin accessibility upon ILC stimulation. Left: number of genes changing expression over 2-fold ($p < 0.05$) after stimulation. Right: number of peaks gained (orange) or lost (blue) after stimulation.

(C) Dendrogram showing hierarchical clustering analysis of ILC gene expression and chromatin accessibility before (black) and after (red) stimulation.

(D) Genome track view of the *Ifng* locus showing RNA-seq, ATAC-seq, H3K27 acetylation, and p300 binding for stimulated and non-stimulated NK cells.

See also Experimental Procedures, Figure S3, and Table S1.

Next, we compared the global views of ILC-lineage identity defined by regulomes versus transcriptomes. Hierarchical clustering of either genome-wide gene expression or chromatin accessibility of ten cell types revealed relationships between bone marrow progenitors (HSCs, CLPs, and MPPs) as well as peripheral mature ILCs (Figure 4C). However, assessment of transcriptomes revealed a different picture of NKp and ILC2p cells than regulomes. The transcriptomes of bone marrow ILC2p and NKp cells are highly correlated with each other and cluster with early progenitors (Figures 4C and S4C, left). On the other hand, comparison of regulomes clustered bone marrow ILC2p cells with differentiated gut ILC2s (Figures 4C and S4C, right). Similarly, bone marrow NKp and iNK cells clustered with mature, splenic NK cells and ILC1s. One explanation for this difference is that ILC regulomes were established prior to terminal differentiation. To test this possibility, we examined the accessible chromatin landscapes of ILC-signature genes such as *Ifng* and Th2 cytokines. Indeed, the majority of lineage-signature REs were already accessible at precursor stages (Figures 4D and 4E), supporting our hypothesis.

To further understand how ILC regulomes are formed during development and how relevant they are to ILC function, we compared REs among mature ILCs (NK and ILC2), ILC precursors (NKp and ILC2p), and CLPs (Figures 5A and 5B). We first identified REs gained and lost during ILC development, dividing them into early and late events (categories A and B for gained REs; categories C and D for lost REs). REs that were gained during ILC development were enriched for the motifs of specific LDTFs. In contrast, REs that were lost during ILC specification were enriched for motifs of early progenitor and myeloid-associated TFs, such as Pu.1 and Spi-B. Remarkably, the transitioning REs, specifically accessible only in precursors, were enriched with motifs of both T-box and GATA families. This observation suggests the existence of a plastic stage prior to final differentiation in which titration of the level of these two TF families could determine differentiated cell identity.

Next, we analyzed the expression level of genes in proximity to differentially accessible REs (Figures 5C and 5D). As expected, we found that the genes associated with regions that only became accessible at the final developmental stage (category A) were also induced late. However, the genes with REs in ILC precursor cells (category B) showed an expression trend similar to category A, suggesting that REs of these genes were

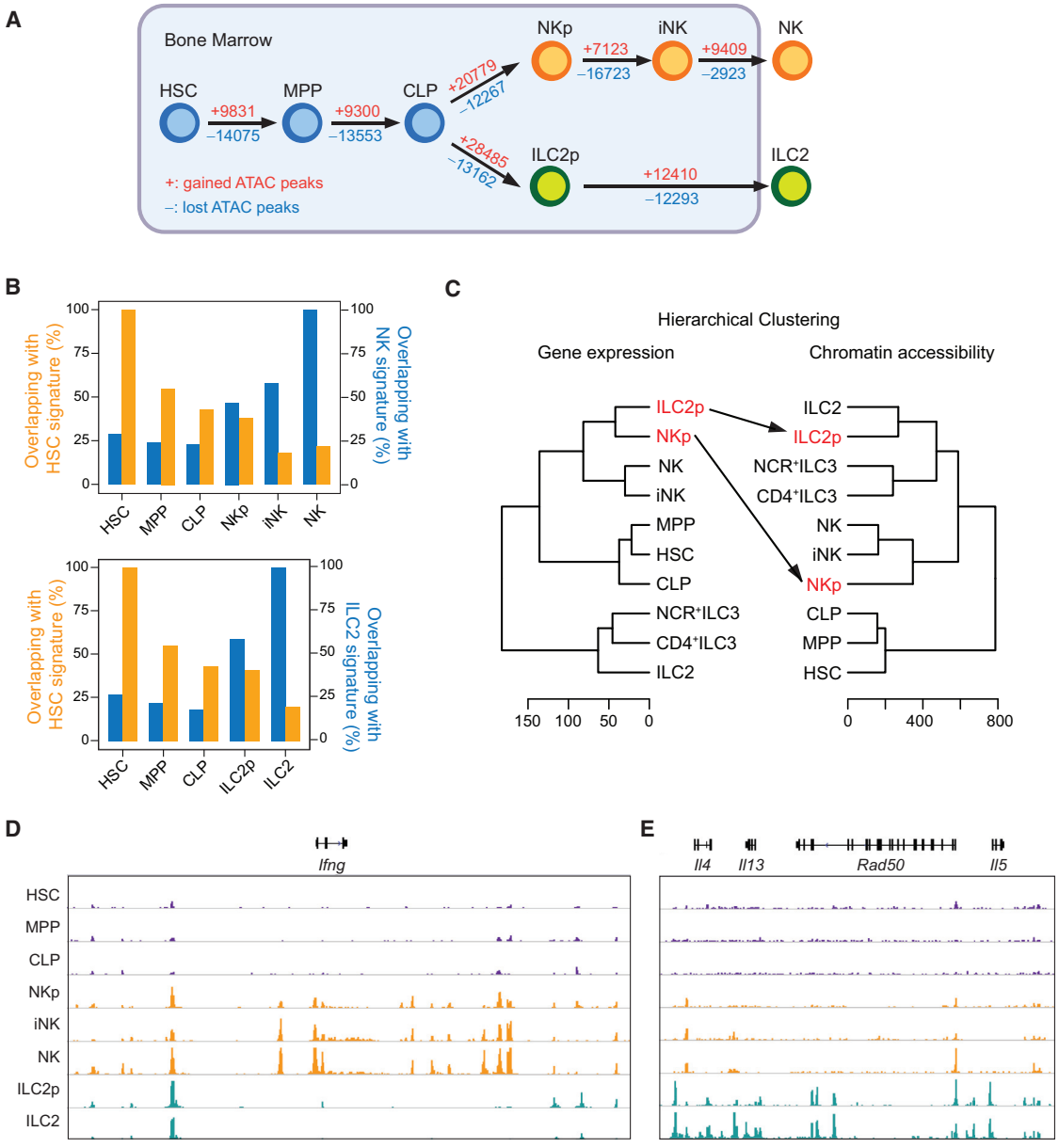

Figure 4. Distinctive ILC Enhancer Landscapes Diverge in Development

(A) Schematic diagram of the ILC developmental stages evaluated by ATAC-seq and RNA-seq. The numbers of ATAC peaks gained or lost during transition determined by the PAPST program (Bible et al., 2015) are shown in red and blue, respectively, along the arrows.

(B) Bar plot illustrating progressive loss of HSC signature (yellow) and reciprocal gain of mature lineage signature (blue) for NK (top) or ILC2 (bottom) during ILC development.

(C) Dendrogram showing hierarchical clustering analysis of ILC gene expression (left) and chromatin accessibility (right) of developing ILCs. Log2-transformed tag counts averaged from replicates were used for calculation of Euclidean distances between two cell types with thresholds of 1 FPKM and 1 RPM for RNA-seq and ATAC-seq datasets, respectively, and were further clustered by the hclust program in R using the ward method.

(D and E) Genome track view of the *Ifng* and *Th2* loci showing early establishment of divergent chromatin landscapes during ILC development.

See also Experimental Procedures, Figure S4, and Table S1.

pre-deposited prior to terminal differentiation. Similarly, among the genes upregulated at the final differentiation stages, over half possessed pre-established REs (Figures 5E, 5F, and S5). These results reinforce the notion that lineage-specific chromatin landscapes diverge early during ILC development.

Relationships between Innate and Adaptive Lymphoid Cells

ILC nomenclature was originally proposed on the basis of effector functions and LDTF expression reflecting cognate T cell subsets. However, unlike ILCs initiating both development

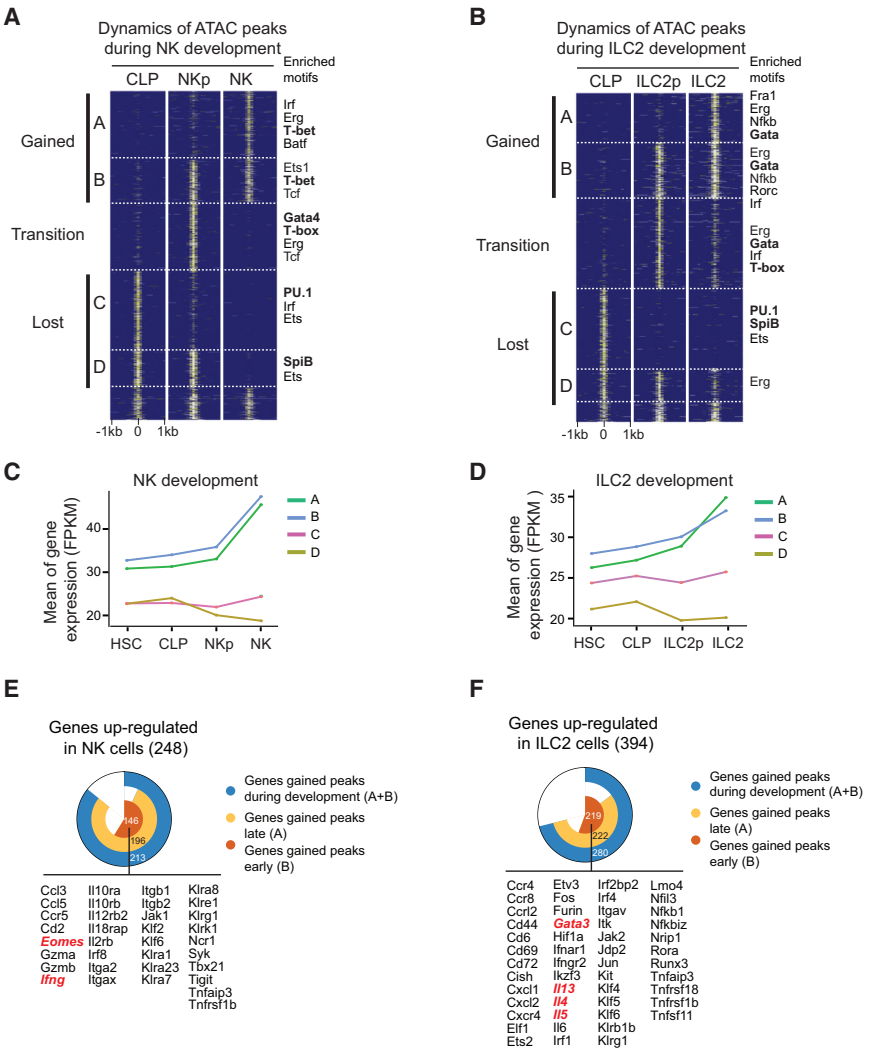

Figure 5. Regulatory Elements of ILC-Signature Genes Are Defined Prior to Maturation

(A and B) Dynamics of regulomes during NK (A) and ILC2 (B) development. ATAC-seq peaks were classified into four categories based on their presence at different developmental stages. A: present in mature ILCs only; B: present in both ILC precursors and mature ILCs; C: present in CLPs only; and D: present in both CLP and ILC precursors. Representative motifs enriched in each group are listed on the right.

(C and D) Mean expression level (FPKM) of genes in proximity to REs categorized in (A) and (B) during ILC development is plotted.

(E and F) REs in proximity to genes upregulated during NK (E) and ILC2 (F) development were evaluated for their timing of acquisition (early versus late). Representative genes that acquire REs early (group 2) are listed.

See also Experimental Procedures, Figure S5, and Table S1.

and differentiation in bone marrow, T cells develop in the thymus and then further differentiate upon stimulation. To understand the relationships between ILC and T cell regulomes, we performed ATAC-seq on ex vivo isolated T cells in healthy mice, including naive and memory $CD8^+$ T cells from bone marrow and naive $CD4^+$ T cells from spleen. For memory/effector $CD4^+$ T cells, we isolated Th17 (GFP^+) cells from the intestine of Il17-GFP mice, using $CCR6^+CD25^-$, $CCR6^-CD25^+$, and $CCR6^-CD25^-$ $CD4^+$ T cells as controls.

To systematically compare the regulatory landscapes of different lineages, we performed hierarchical clustering on ATAC-seq similarity of in-house and published ATAC-seq (Figure 6). The latter dataset includes macrophages, microglia, and dendritic cells, as well as NK cells. This analysis revealed several features that suggest how regulomes can be useful for exploring cell identity. First, the analysis recapitulated our previous findings of the similarity between ILC precursors and their differentiated progeny (Figure 4C). Second, the analysis illustrated the relatively low impact of environment in determining characteristic regulomes of type 1 ILCs in different tissues (liver, bone marrow, spleen), which clustered together irrespective of the organ from which they were isolated. Third, the analysis showed ILCs (clade 1) having a closer relationship with T cells (clade 2) than with B cells and hematopoietic progenitors (clade 3) or with myeloid cells (clade 4). Finally, the results reinforced the current view of ILCs as distinct groups of cells with well-defined markers.

ILC and T Helper Chromatin Landscapes Converge upon Infection

Given the clustering of T cells and ILCs in healthy hosts, we next compared their chromatin landscapes following infection. Naive $CD4^+$ T cells require potent polarizing stimuli for effector differentiation; however, the similarity of effector ILC and Th cell transcriptomes and regulomes has not been assessed. To resolve this issue, we sought to obtain ILCs and T cells subjected to the same environment by infecting mice with *Nippostrongylus brasiliensis*, a parasitic nematode provoking a Th2-dominant immune response (Finkelman et al., 2004). Both ILC2 and Th2 cells were enriched in lungs after 10 days of infection and then isolated for ATAC-seq and RNA-seq analysis (Figure 7A). By comparing REs of Th2-related genes (*Il4*, *Il5*, *Il9*, *Il10*, and *Il13*) in *N. brasiliensis*-infected ILC2 and Th2 cells, we were struck by the similarities of the chromatin landscapes between these two cells, in spite of their differences prior to infection (Figure 7B). Notably, the majority of these REs were generated de novo in *N. brasiliensis*-infected Th2 cells compared to ILCs in which more modest changes were evident upon infection. Genome-wide analysis of accessible REs in *N. brasiliensis*-induced Th2 cells revealed that these cells lost over half of naive signature REs and two-thirds of Th2 REs

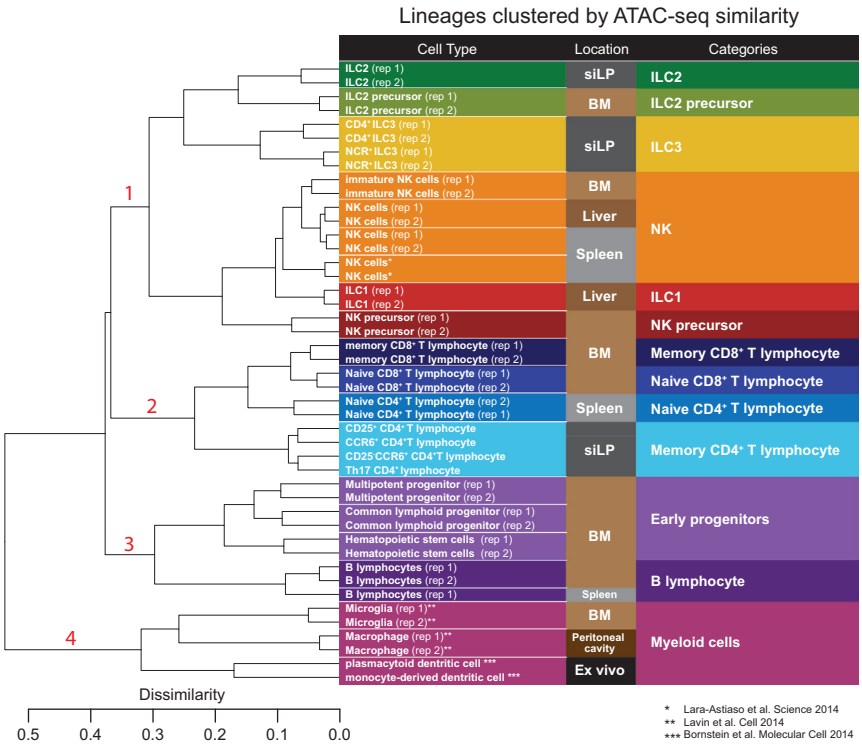

Figure 6. Relationships between Innate and Adaptive Cell Regulomes

Dendrogram showing unbiased hierarchical clustering analysis of lineage relationships based on 37 in-house and 8 previous published ATAC-seq data. Categories of cell types and tissue location from which the cells were harvested are indicated on the right and colored accordingly. The distance on the scale implies the dissimilarity (1 – Pearson correlation coefficient) between two individual subjects. Log2-transformed tag counts were used for calculation of dissimilarity between two cell types with a threshold of 1 RPM. BM, bone marrow.

See also Supplemental Experimental Procedures.

were newly acquired (Figure 7C). Among these Th2-acquired REs, over 70% were also detectable in ILC2s, demonstrating that Th2 cells gained a large portion of ILC2 regulomes upon infection. Consistently, pairwise comparison of gene expression among type 2 subsets, including ILC2p from bone marrow, ILC2 from small intestine, and both ILC2 and Th2 cells from lung of *N. brasiliensis*-infected mice, revealed minimal expression difference between *N. brasiliensis*-infected ILC2 and Th2 cells (Figure 7D). In contrast, the maximum difference in gene expression was observed between Th2 cells and naive $CD4^+$ T cells. Hierarchical clustering emphasized the difference between the pre-established ILC and naive $CD4^+$ T cell regulomes, although infection led to a convergence of circuitry (Figure 7E). To better define the basis of the convergence, we performed gene ontology analysis using GREAT (Genomic Regions Enrichment of Annotations Tool) (Ashburner et al., 2000; McLean et al., 2010) to identify genes that shared ATAC accessibility in infected Th2 and ILC2 cells. Comparison of accessible peaks present in both cell types relative to the background of the whole genome revealed significant enrichment for several immune response-related molecular functions. An additional explanation for the convergence of Th2 and ILC2 regulomes might be similar changes in metabolic state; however, we found no significant enrichment in general metabolism or cell-cycle terms (Figure S6). Therefore, the environmental impact of infection was able to synchronize gene regulation in ILC2 and Th2 cells, despite the greater impact on the latter. This implies substantial overlap of their regulatory networks even though they were established through distinct routes.

DISCUSSION

In the present study, we sought to gain insight into the biology of ILCs by characterizing regulomes for the prototypic subsets and determining their roles in gene expression. Our data reveal how ILC regulomes "mature" progressively during development such that many key loci are primed prior to terminal differentiation. As a consequence, these loci are only moderately impacted by stimulation in vitro and in vivo. This contrasts with $CD4^+$ Th cells, which undergo dramatic chromatin remodeling upon activation. However, during the course of infection, the regulomes of $CD4^+$ T cells and ILCs closely approximate one another, arguing for substantial sharing of mechanisms underlying regulation of lineage-specific functions.

Genomic Views of ILC Classification

With the expanding recognition of innate lymphocyte subsets, a classification of ILCs was proposed based on their analogy with $CD4^+$ Th cell subsets. However, the precise distinctions between conventional NK cells and ILC1s have been unclear and the heterogeneity of ILC3s has challenged simple classification. The identification of ILC3s expressing T-bet and the overlapping roles of LDTFs in ILC differentiation further complicate the picture (Tindemans et al., 2014). Although the present classification posits that ILCs such as T helper cells are specified to distinct "lineages," the ability to comprehensively map the regulatory landscape of ILCs raises the question of how the current functional classification compares to a genomic perspective. The five recognized major subsets of ILCs, conventional NK, ILC1, ILC2, NCR^+ ILC3, and $CD4^+$ ILC3 cells, can be discerned by chromatin landscapes since they cluster in three main groups, although differences between NK and ILC1 cells and ILC3s are also apparent. The mechanisms establishing the similarities and differences in chromatin landscapes will be important to discern in the future, and the comprehensive regulomes defined in the current work will facilitate this endeavor.

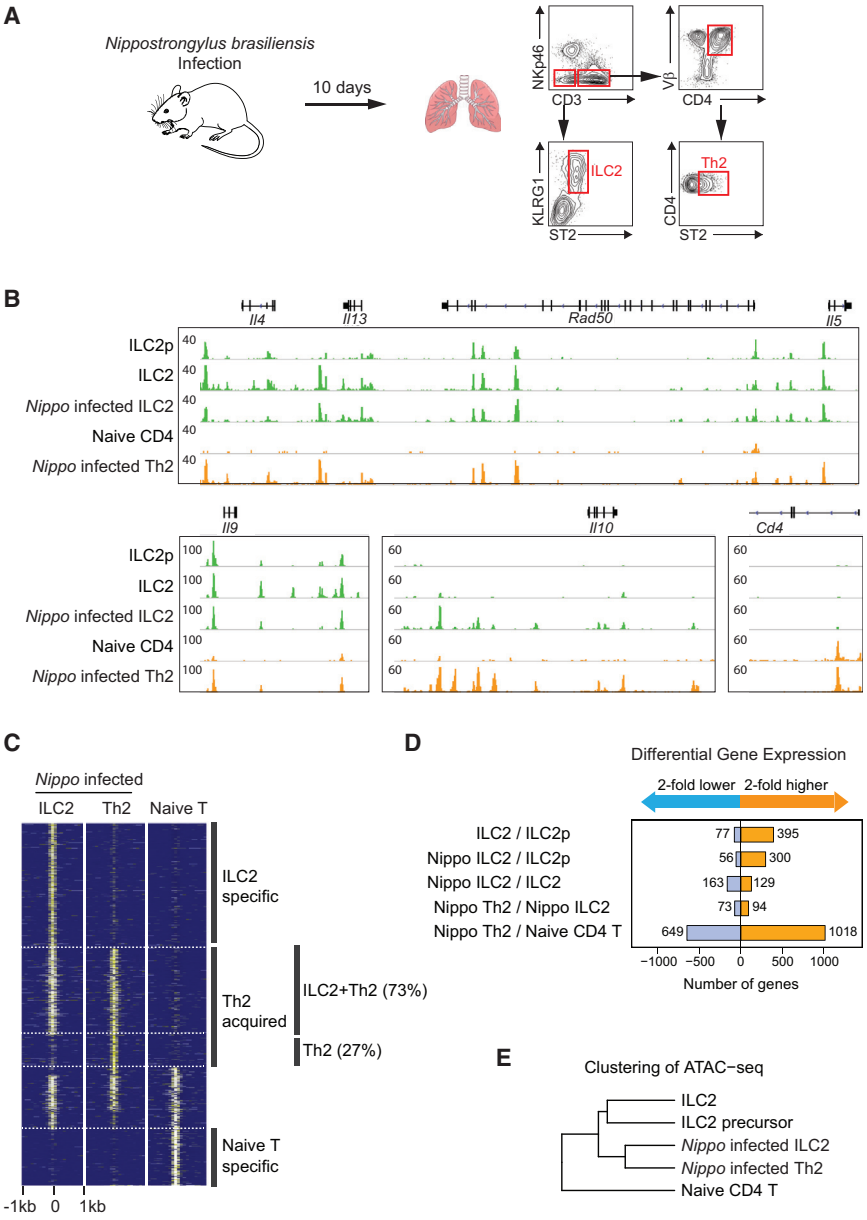

Figure 7. Similarity of ILC2 and Th2 Regulomes upon Infection

(A) Schematic illustration of experimental design. Lung cells from Foxp3-GFP mice infected with *N. brasiliensis* were sorted by flow cytometry. In the GFP-negative fraction, Th2 cells were sorted as $CD3\varepsilon^{+}V\beta^{+}CD4^{+}ST2^{+}$ cells, whereas ILC2 cells were sorted as $CD3\varepsilon^{-}NKp46^{-}KLRG1^{+}ST2^{+}$ cells. Purity of sorted cells ranges from 95% to 99% post sort.

(B) Representative examples of ATAC-seq signals in type 2 innate and adaptive cells at loci including Th2 cytokines *Il9* and *Il10*. *Cd4* is a lineage marker that distinguishes ILC2 and Th2 cells.

(C) Comparison of ATAC-seq signals at signature REs in infected ILC2, Th2, and naive $CD4^{+}$ T cells. A substantial portion of Th2 ATAC-seq peaks acquired upon infection (73%) was shared with infected ILC2.

See also Table S1 for accessible regions.

(D) Pairwise comparison of differential gene expression among type 2 innate and adaptive cells.

(E) Dendrogram showing hierarchical clustering of type 2 innate and adaptive cell regulomes to evaluate their similarities. Log2-transformed tag counts averaged from replicates were used for calculation of Euclidean distances between two cell types with thresholds of 1 FPKM and 1 RPM for RNA-seq and ATAC-seq datasets, respectively, and were further clustered by the hclust program in R using the ward method.

See also Supplemental Experimental Procedures.

Underpinnings of Rapid Effector Responses in ILCs

A general characteristic of ILCs is their rapid and selective responses to infection. Locksley and colleagues first recognized the accessibility of the *Ifng* promoter in NK cells, as measured by histone acetylation (Stetson et al., 2003). Consistently, our global analysis revealed that the REs of effector gene loci were accessible in resting ILCs and changed little following activation, despite the increase of enhancer activity measured by p300 and histone acetylation. A striking finding of our work is that most of these REs are pre-formed in ILC precursors and become accessible in a stepwise manner during development. It should be noted that chromatin accessibility detected by ATAC-seq includes promoters, silencers, and insulators as well as enhancers; however, we would argue that a significant proportion of ATAC-accessible regions are enhancers, due to the fact that 40% of all ATAC peaks in NK cells are bound by p300, a useful proxy for enhancer activity in previous studies (Visel et al., 2009) despite its functional redundancy with other co-activators (e.g., CREB-binding protein, Pcaf).

Environment versus Ontogeny of ILC Subsets

ILCs are important for barrier function, where they are exposed to diverse exogenous and endogenous environmental stimuli; consequently, ILCs exhibit distinct functionalities in different tissues. This correlates well with the recently reported distinctive transcriptomes of intestinal ILCs (Robinette et al., 2015). In other innate cells, such as macrophages, environment also controls both gene expression and enhancers to define tissue-specific macrophage identities (Gosselin et al., 2014; Lavin et al., 2014). In view of these previous observations, we were struck by the contrast in viewing ILC identity by transcriptomes versus regulomes. ILC regulomes appear to be less sensitive to tissue localization and primarily reflect lineage relationships. In particular, regulomes define the lineage segregation between ILC2s and ILC3s better than transcriptome analyses. Also, comparison of transcriptomes revealed similarities between ILC2 and NK precursors, whereas inspection of regulomes revealed

more similarities between precursors and their offspring. Understanding the factors that establish chromatin landscapes will be revealing; presumably, this is the consequence of the action of TFs that are either induced or activated during development. A better understanding of the regulatory logic of these developmental circuits will be important in elucidating the creation of these landscapes.

Mechanisms Allowing ILC Plasticity

Although selective cytokine production is a major feature of the current classification of ILCs, substantial phenotypic plasticity has recently become evident (Bernink et al., 2013; Cella et al., 2009; Huang et al., 2015; Kearley et al., 2015; Klose et al., 2013; Serafini et al., 2015). Signature cytokine loci are most accessible in the expected subsets. However, it is clear that there are elements that are broadly accessible in all subsets. For instance, CNS-22, an element previously shown to be involved in activation-specific IFN-γ induction in T cells (Balasubramani et al., 2014), was accessible in all ILCs, including those not making this cytokine. Perhaps such elements represent "seed" enhancers (Factor et al., 2014), which have permissive actions on the general organization of the locus and precede selective, high-level IFN-γ expression. Even more notable is that the broad accessibility of loci encoding LDTFs across ILCs provides a mechanism for phenotypic flexibility in the context of permitting rapid responses. Alternatively, the accessibility of loci encoding LDTFs provides opportunities for cross-regulation. Taken together, the data make clear that despite mechanisms allowing selective cytokine production, multiple means exist to allow plasticity and flexible expression of effector genes.

T Cells and ILCs: Regulomes Converge following Infection

The existing classification of ILCs and T helper cells implies functional relationships between them. However, the extent to which they truly share mechanisms to regulate common batteries of effector genes remains an important question that has not been previously examined. In principle, this question can be addressed both in terms of development (ontogeny) and evolution (phylogeny). From the view of development, our data indicate that ILCs are instructed in the bone marrow and undergo a stepwise process of specification. The unbiased view of the regulomes of naive $CD4^+$ T cells would lead one to believe that they are distinct from ILCs, suggesting that their ability to acquire effector functions might involve mechanisms rather distinct from ILCs. This is consistent with a reasonably clear distinction between ILC and T cell development (Shih et al., 2014). Nonetheless, following infection, the regulomes of ILCs and T cells approximate each other to a remarkable degree. This suggests that mechanisms underlying selective effector gene expression are shared between T cells and ILCs and may be evolutionarily ancient. Although we know relatively little about the evolution of lymphocytes, the existence of two distinct modes of antigen-specific recognition in lymphocytes in vertebrate evolution (Hirano et al., 2011) could suggest that "innate" lymphoid cells may have preceded T cells evolutionarily (Serafini et al., 2015). Precisely why T cell development is associated with the absence of a pre-primed or poised regulome is not clear; however, this clearly allows for more room to control the system in which massive clonal expansion occurs along with acquisition of effector functions, rather than pre-existing functionalities during infection.

Conclusion

The discovery of diverse, functionally specialized ILC subsets represents a major advance in our knowledge of how the immune system copes with infection, inflammation, tissue repair, and metabolic homeostasis. The apparent functional symmetry of the innate and adaptive systems makes efforts to understand the molecular relationship between ILCs and T cells of great interest. Our elucidation of the regulomes of ILCs and T cells provides insights into the genomic mechanisms that specify functions of different lineages. Deciphering the precise nature of circuits that shape the regulomes of ILC and T cells is an exciting area for future work.

EXPERIMENTAL PROCEDURES

Mice

Female wild-type C57BL/6J, Foxp3-GFP, and Il17-GFP mice (6–12 weeks old) were purchased from the Jackson Laboratory. All animal studies were performed according to NIH guidelines for the use and care of live animals and were approved by the Institutional Animal Care and Use Committee of the National Institute of Arthritis and Musculoskeletal and Skin Diseases (NIAMS).

Cell Isolation

NK cells were isolated from spleen and liver; ILC1 cells were isolated from liver; Il17-GFP^+ Th17, ILC2s, $CD4^+$ ILC3, and NCR^+ ILC3 cells were isolated from siLP; HSCs and CLP, NKp, immature NK, and ILC2p cells were isolated from bone marrow; and *N. brasiliensis*-induced ILC2 and Th2 cells were isolated from lung. Cells from bone marrow, liver, and spleen were obtained by mechanical disruption. Cells from lung were isolated after incubating lung fragments with 0.5 mg/ml Liberase TL (Roche) for 1 hr followed by purification with 40% Percoll (GE Healthcare) (Meylan et al., 2014). Cells from siLP were isolated after incubating fine-cut intestine in HBSS with 0.5 mg/ml DNase I (Roche) and 0.25 mg/ml Liberase TL followed by filtering with a 100-μm cell strainer and purification with 40% Percoll (Sciumé et al., 2012). Isolated cells were further sorted as described previously. See Supplemental Experimental Procedures for the antibodies used.

In Vitro Stimulation

All cells were stimulated in RPMI medium with 10% (vol/vol) FCS (Invitrogen), 2 mM glutamine (Invitrogen), 100 IU/ml penicillin (Invitrogen), 0.1 mg/ml streptomycin (Invitrogen), 20 mM HEPES buffer (pH 7.2–7.5) (Invitrogen), and 2 mM β-mercaptoethanol (Sigma-Aldrich). NK cells were treated with 1,000 U/ml IL-2 and 10 ng/ml IL-12 (R&D Systems) for 6 hr; ILC2 cells were treated with 50 ng/ml IL-25 (BioLegend) and 50 ng/ml IL-33 (BioLegend) for 4 hr; and NCR^+ ILC3 cells were treated with IL-23 (50 ng/ml; R&D Systems) for 4 hr.

In Vivo ILC2 and Th2 Induction

Mice of at least 8 weeks of age were infected with 500 infective third-stage *N. brasiliensis* by subcutaneous injection. Cells from lungs were isolated after 10 days of infection. Staining and sorting strategy of Th2 and ILC2 cells were as described in Figure 7.

RNA-Seq

RNA-seq was performed as described previously with slight modification (Hirahara et al., 2015). Total RNA was prepared from approximately 30,000–50,000 cells by using TRIzol following the manufacturer's protocol (Life Technologies). Total RNA was subsequently processed to generate an mRNA-seq library using a TruSeq SR mRNA sample prep kit (FC-122-1001; Illumina). The libraries were sequenced for 50 cycles (single read) with a HiSeq 2000 or HiSeq

2500 (Illumina). Raw sequencing data were processed with CASAVA 1.8.2 (Illumina; Bentley et al., 2008) to generate FastQ files.

RNA-Seq Analysis

Sequence reads were mapped onto mouse genome build mm9 using TopHat 2.1.0 (Trapnell et al., 2012). Gene expression values (FPKM; fragments per kilobase exon per million mapped reads) were calculated with Cufflinks 2.2.1 (Trapnell et al., 2012). BigWig tracks were generated from Bam files and converted into bedGraph format using bedtools (Quinlan and Hall, 2010). These were further reformatted with the UCSC tool bedGraphToBigWig. The differential gene expression was determined by DEseq using 2-fold change, with p value <0.05 as threshold (Anders and Huber, 2010). Downstream analyses and heatmaps were performed with R 3.0.1 (R Core Team, 2014) and custom R programs.

See also Supplemental Experimental Procedures.

ATAC-Seq

ATAC-seq was performed according to a published protocol (Buenrostro et al., 2013) with minor modification. Fifty thousand cells were pelleted and washed with 50 μl 1× PBS, followed by treatment with 50 μl lysis buffer (10 mM Tris-HCl [pH 7.4], 10 mM NaCl, 3 mM $MgCl_2$, 0.1% IGEPAL CA-630). After pelleting the nuclei by centrifuging at 500 × *g* for 10 min, the pellets were re-suspended in a 40-μl transposition reaction with 2 μl Tn5 transposase (FC-121-1030; Illumina) to tag and fragmentalize accessible chromatin. The reaction was incubated at 37°C with shaking at 300 rpm for 30 min. The fragmentalized DNAs were then purified using a QIAGEN MinElute kit and amplified with 10 or 11 cycles of PCR based on the amplification curve. Once the libraries were purified using a QIAGEN PCR cleanup kit, they were further sequenced for 50 cycles (paired-end reads) on a HiSeq 2500.

ATAC-Seq Analysis

ATAC-seq reads from two biological replicates for each sample were mapped to the mouse genome (mm9 assembly) using Bowtie 0.12.8 (Langmead et al., 2009). In all cases, redundant reads were removed using FastUniq (Xu et al., 2012), and customized Python scripts were used to calculate the fragment length of each pair of uniquely mapped paired-end (PE) reads. The fragment sizes distribute similar to previously published data (data not shown). Only one mapped read to each unique region of the genome that was less than 175 bp was kept and used in peak calling. Regions of open chromatin were identified by MACS (version 1.4.2) (Zhang et al., 2008) using a p-value threshold of 1×10^{-5}. Only regions called in both replicates were used in downstream analysis. Peak intensities ("tags" column) were normalized as tags per 10 million reads (RP10M) in the original library. Downstream analysis and heatmap generation were performed with the Hypergeometric Optimization of Motif EnRichment program (HOMER) version 4.8 (Heinz et al., 2010) and R 3.0.1 (R Core Team, 2014).

See also Supplemental Experimental Procedures.

Chromatin Immunoprecipitation Sequencing

ChIP-seq was performed using ex vivo purified NK cells without or with cytokine stimulation. At least 10 million cells were used for transcription factor ChIP, and 2 million cells were used for histone mark ChIP. After chemically cross-linking cells, chromatin was fragmented by sonication and immunoprecipitated by anti-H3K27Ac (ab4729; Abcam), anti-p300 (sc585; Santa Cruz), or anti-T-bet (sc21003; Santa Cruz). After recovering purified DNA, 10 ng or more of DNA was used to generate libraries according to the vendor's manual for the Illumina platform (E6240S/L; New England BioLabs). Illumina HiSeq 2500 (H3K27Ac, T-bet) or Genome Analyzer II (p300) was used for 50-cycle single-read sequencing. SICER (K27Ac; Zang et al., 2009) or MACS 1.4.2 (T-bet, p300) was used for peak calling using the reference genome mm9.

ACCESSION NUMBERS

The ATAC-seq, RNA-seq, and ChIP-seq data have been deposited in the GEO: GSE77695.

SUPPLEMENTAL INFORMATION

Supplemental Information includes Supplemental Experimental Procedures, six figures, and one table and can be found with this article online at http://dx.doi.org/10.1016/j.cell.2016.04.029.

AUTHOR CONTRIBUTIONS

H.-Y.S. and G.S. designed the project and wrote the manuscript. H.-Y.S., G.S., and Y.M. performed and interpreted all the experiments. H.-Y.S. performed ATAC-seq experiments and computational analyses. Y.M. performed RNA-seq experiments. Y.K. performed ChIP-seq experiments. J.F.U. and L.G. helped with *N. brasiliensis* infection experiments. H.-W.S., S.R.B., and F.P.D. helped with genomic data processing and analyses. Y.K. and F.P.D. contributed to data interpretation and manuscript editing. J.J.O. contributed to project design, data interpretation, and manuscript writing.

ACKNOWLEDGMENTS

We thank Drs. Y. Belkaid, K. Zhao, V. Sartorelli, J. Zhu, I. Fraser, and A. Pohoolek for critically reading this manuscript. We also thank G. Gutierrez-Cruz (Genome Analysis Core Facility, NIAMS) and J. Simone, J. Lay, and K. Tinsley (Flow Cytometry Section, NIAMS) for their technical support. This study utilized the high-performance computational capabilities of the Biowulf Linux cluster at the NIH. This work was supported by the Intramural Research Programs of the NIAMS.

Received: January 21, 2016
Revised: March 17, 2016
Accepted: April 6, 2016
Published: May 5, 2016

REFERENCES

Anders, S., and Huber, W. (2010). Differential expression analysis for sequence count data. Genome Biol. *11*, R106.

Artis, D., and Spits, H. (2015). The biology of innate lymphoid cells. Nature *517*, 293–301.

Ashburner, M., Ball, C.A., Blake, J.A., Botstein, D., Butler, H., Cherry, J.M., Davis, A.P., Dolinski, K., Dwight, S.S., Eppig, J.T., et al.; The Gene Ontology Consortium (2000). Gene ontology: tool for the unification of biology. Nat. Genet. *25*, 25–29.

Balasubramani, A., Mukasa, R., Hatton, R.D., and Weaver, C.T. (2010). Regulation of the Ifng locus in the context of T-lineage specification and plasticity. Immunol. Rev. *238*, 216–232.

Balasubramani, A., Winstead, C.J., Turner, H., Janowski, K.M., Harbour, S.N., Shibata, Y., Crawford, G.E., Hatton, R.D., and Weaver, C.T. (2014). Deletion of a conserved *cis*-element in the Ifng locus highlights the role of acute histone acetylation in modulating inducible gene transcription. PLoS Genet. *10*, e1003969.

Barton, K., Muthusamy, N., Fischer, C., Ting, C.N., Walunas, T.L., Lanier, L.L., and Leiden, J.M. (1998). The Ets-1 transcription factor is required for the development of natural killer cells in mice. Immunity *9*, 555–563.

Bentley, D.R., Balasubramanian, S., Swerdlow, H.P., Smith, G.P., Milton, J., Brown, C.G., Hall, K.P., Evers, D.J., Barnes, C.L., Bignell, H.R., et al. (2008). Accurate whole human genome sequencing using reversible terminator chemistry. Nature *456*, 53–59.

Bernink, J.H., Peters, C.P., Munneke, M., te Velde, A.A., Meijer, S.L., Weijer, K., Hreggvidsdottir, H.S., Heinsbroek, S.E., Legrand, N., Buskens, C.J., et al. (2013). Human type 1 innate lymphoid cells accumulate in inflamed mucosal tissues. Nat. Immunol. *14*, 221–229.

Bible, P.W., Kanno, Y., Wei, L., Brooks, S.R., O'Shea, J.J., Morasso, M.I., Loganantharaj, R., and Sun, H.W. (2015). PAPST, a user friendly and powerful Java platform for ChIP-seq peak co-localization analysis and beyond. PLoS ONE *10*, e0127285.

Bornstein, C., Winter, D., Barnett-Itzhaki, Z., David, E., Kadri, S., Garber, M., and Amit, I. (2014). A negative feedback loop of transcription factors specifies alternative dendritic cell chromatin states. Mol. Cell *56*, 749–762.

Buenrostro, J.D., Giresi, P.G., Zaba, L.C., Chang, H.Y., and Greenleaf, W.J. (2013). Transposition of native chromatin for fast and sensitive epigenomic profiling of open chromatin, DNA-binding proteins and nucleosome position. Nat. Methods *10*, 1213–1218.

Cella, M., Fuchs, A., Vermi, W., Facchetti, F., Otero, K., Lennerz, J.K., Doherty, J.M., Mills, J.C., and Colonna, M. (2009). A human natural killer cell subset provides an innate source of IL-22 for mucosal immunity. Nature *457*, 722–725.

Chiossone, L., Chaix, J., Fuseri, N., Roth, C., Vivier, E., and Walzer, T. (2009). Maturation of mouse NK cells is a 4-stage developmental program. Blood *113*, 5488–5496.

Constantinides, M.G., McDonald, B.D., Verhoef, P.A., and Bendelac, A. (2014). A committed precursor to innate lymphoid cells. Nature *508*, 397–401.

De Obaldia, M.E., and Bhandoola, A. (2015). Transcriptional regulation of innate and adaptive lymphocyte lineages. Annu. Rev. Immunol. *33*, 607–642.

Diefenbach, A., Colonna, M., and Koyasu, S. (2014). Development, differentiation, and diversity of innate lymphoid cells. Immunity *41*, 354–365.

Eberl, G., Colonna, M., Di Santo, J.P., and McKenzie, A.N.J. (2015). Innate lymphoid cells: a new paradigm in immunology. Science *348*, aaa6566.

Ebihara, T., Song, C., Ryu, S.H., Plougastel-Douglas, B., Yang, L., Levanon, D., Groner, Y., Bern, M.D., Stappenbeck, T.S., Colonna, M., et al. (2015). Runx3 specifies lineage commitment of innate lymphoid cells. Nat. Immunol. *16*, 1124–1133.

Factor, D.C., Corradin, O., Zentner, G.E., Saiakhova, A., Song, L., Chenoweth, J.G., McKay, R.D., Crawford, G.E., Scacheri, P.C., and Tesar, P.J. (2014). Epigenomic comparison reveals activation of "seed" enhancers during transition from naive to primed pluripotency. Cell Stem Cell *14*, 854–863.

Fathman, J.W., Bhattacharya, D., Inlay, M.A., Seita, J., Karsunky, H., and Weissman, I.L. (2011). Identification of the earliest natural killer cell-committed progenitor in murine bone marrow. Blood *118*, 5439–5447.

Finkelman, F.D., Shea-Donohue, T., Morris, S.C., Gildea, L., Strait, R., Madden, K.B., Schopf, L., and Urban, J.F., Jr. (2004). Interleukin-4- and interleukin-13-mediated host protection against intestinal nematode parasites. Immunol. Rev. *201*, 139–155.

Gosselin, D., Link, V.M., Romanoski, C.E., Fonseca, G.J., Eichenfield, D.Z., Spann, N.J., Stender, J.D., Chun, H.B., Garner, H., Geissmann, F., and Glass, C.K. (2014). Environment drives selection and function of enhancers controlling tissue-specific macrophage identities. Cell *159*, 1327–1340.

Heinz, S., Benner, C., Spann, N., Bertolino, E., Lin, Y.C., Laslo, P., Cheng, J.X., Murre, C., Singh, H., and Glass, C.K. (2010). Simple combinations of lineage-determining transcription factors prime *cis*-regulatory elements required for macrophage and B cell identities. Mol. Cell *38*, 576–589.

Heinz, S., Romanoski, C.E., Benner, C., and Glass, C.K. (2015). The selection and function of cell type-specific enhancers. Nat. Rev. Mol. Cell Biol. *16*, 144–154.

Hirahara, K., Onodera, A., Villarino, A.V., Bonelli, M., Sciumè, G., Laurence, A., Sun, H.-W., Brooks, S.R., Vahedi, G., Shih, H.-Y., et al. (2015). Asymmetric action of STAT transcription factors drives transcriptional outputs and cytokine specificity. Immunity *42*, 877–889.

Hirano, M., Das, S., Guo, P., and Cooper, M.D. (2011). The evolution of adaptive immunity in vertebrates. In Advances in Immunology, *Volume 109*, Alt F.W., ed. (Academic), pp. 125–157.

Hoyler, T., Klose, C.S.N., Souabni, A., Turqueti-Neves, A., Pfeifer, D., Rawlins, E.L., Voehringer, D., Busslinger, M., and Diefenbach, A. (2012). The transcription factor GATA-3 controls cell fate and maintenance of type 2 innate lymphoid cells. Immunity *37*, 634–648.

Huang, Y., Guo, L., Qiu, J., Chen, X., Hu-Li, J., Siebenlist, U., Williamson, P.R., Urban, J.F., Jr., and Paul, W.E. (2015). IL-25-responsive, lineage-negative KLRG1(hi) cells are multipotential 'inflammatory' type 2 innate lymphoid cells. Nat. Immunol. *16*, 161–169.

Kang, J., and Malhotra, N. (2015). Transcription factor networks directing the development, function, and evolution of innate lymphoid effectors. Annu. Rev. Immunol. *33*, 505–538.

Kearley, J., Silver, J.S., Sanden, C., Liu, Z., Berlin, A.A., White, N., Mori, M., Pham, T.-H., Ward, C.K., Criner, G.J., et al. (2015). Cigarette smoke silences innate lymphoid cell function and facilitates an exacerbated type I interleukin-33-dependent response to infection. Immunity *42*, 566–579.

Kim, C.C., and Lanier, L.L. (2013). Beyond the transcriptome: completion of act one of the Immunological Genome Project. Curr. Opin. Immunol. *25*, 593–597.

Klose, C.S.N., and Diefenbach, A. (2014). Transcription factors controlling innate lymphoid cell fate decisions. Curr. Top. Microbiol. Immunol. *381*, 215–255.

Klose, C.S.N., Kiss, E.A., Schwierzeck, V., Ebert, K., Hoyler, T., d'Hargues, Y., Göppert, N., Croxford, A.L., Waisman, A., Tanriver, Y., and Diefenbach, A. (2013). A T-bet gradient controls the fate and function of CCR6^{-}RORγt^{+} innate lymphoid cells. Nature *494*, 261–265.

Langmead, B., Trapnell, C., Pop, M., and Salzberg, S.L. (2009). Ultrafast and memory-efficient alignment of short DNA sequences to the human genome. Genome Biol. *10*, R25.

Lara-Astiaso, D., Weiner, A., Lorenzo-Vivas, E., Zaretsky, I., Jaitin, D.A., David, E., Keren-Shaul, H., Mildner, A., Winter, D., Jung, S., et al. (2014). Chromatin state dynamics during blood formation. Science *345*, 943–949.

Lavin, Y., Winter, D., Blecher-Gonen, R., David, E., Keren-Shaul, H., Merad, M., Jung, S., and Amit, I. (2014). Tissue-resident macrophage enhancer landscapes are shaped by the local microenvironment. Cell *159*, 1312–1326.

Lohoff, M., Duncan, G.S., Ferrick, D., Mittrücker, H.W., Bischof, S., Prechtl, S., Röllinghoff, M., Schmitt, E., Pahl, A., and Mak, T.W. (2000). Deficiency in the transcription factor interferon regulatory factor (IRF)-2 leads to severely compromised development of natural killer and T helper type 1 cells. J. Exp. Med. *192*, 325–336.

McLean, C.Y., Bristor, D., Hiller, M., Clarke, S.L., Schaar, B.T., Lowe, C.B., Wenger, A.M., and Bejerano, G. (2010). GREAT improves functional interpretation of cis-regulatory regions. Nat. Biotechnol. *28*, 495–501.

Meylan, F., Hawley, E.T., Barron, L., Barlow, J.L., Penumetcha, P., Pelletier, M., Sciumè, G., Richard, A.C., Hayes, E.T., Gomez-Rodriguez, J., et al. (2014). The TNF-family cytokine TL1A promotes allergic immunopathology through group 2 innate lymphoid cells. Mucosal Immunol. *7*, 958–968.

Quinlan, A.R., and Hall, I.M. (2010). BEDTools: a flexible suite of utilities for comparing genomic features. Bioinformatics *26*, 841–842.

Rankin, L.C., Groom, J.R., Chopin, M., Herold, M.J., Walker, J.A., Mielke, L.A., McKenzie, A.N., Carotta, S., Nutt, S.L., and Belz, G.T. (2013). The transcription factor T-bet is essential for the development of NKp46^{+} innate lymphocytes via the Notch pathway. Nat. Immunol. *14*, 389–395.

R Core Team (2014). R: A Language and Environment for Statistical Computing (R Foundation for Statistical Computing).

Robinette, M.L., Fuchs, A., Cortez, V.S., Lee, J.S., Wang, Y., Durum, S.K., Gilfillan, S., Colonna, M., Shaw, L., Yu, B., et al.; Immunological Genome Consortium (2015). Transcriptional programs define molecular characteristics of innate lymphoid cell classes and subsets. Nat. Immunol. *16*, 306–317.

Rosmaraki, E.E., Douagi, I., Roth, C., Colucci, F., Cumano, A., and Di Santo, J.P. (2001). Identification of committed NK cell progenitors in adult murine bone marrow. Eur. J. Immunol. *31*, 1900–1909.

Sciumé, G., Hirahara, K., Takahashi, H., Laurence, A., Villarino, A.V., Singleton, K.L., Spencer, S.P., Wilhelm, C., Poholek, A.C., Vahedi, G., et al. (2012). Distinct requirements for T-bet in gut innate lymphoid cells. J. Exp. Med. *209*, 2331–2338.

Serafini, N., Vosshenrich, C.A.J., and Di Santo, J.P. (2015). Transcriptional regulation of innate lymphoid cell fate. Nat. Rev. Immunol. *15*, 415–428.

Shay, T., and Kang, J. (2013). Immunological Genome Project and systems immunology. Trends Immunol. *34*, 602–609.

Shih, H.-Y., Sciumè, G., Poholek, A.C., Vahedi, G., Hirahara, K., Villarino, A.V., Bonelli, M., Bosselut, R., Kanno, Y., Muljo, S.A., and O'Shea, J.J. (2014). Transcriptional and epigenetic networks of helper T and innate lymphoid cells. Immunol. Rev. *261*, 23–49.

Sonnenberg, G.F., and Artis, D. (2015). Innate lymphoid cells in the initiation, regulation and resolution of inflammation. Nat. Med. *21*, 698–708.

Spits, H., Artis, D., Colonna, M., Diefenbach, A., Di Santo, J.P., Eberl, G., Koyasu, S., Locksley, R.M., McKenzie, A.N., Mebius, R.E., et al. (2013). Innate lymphoid cells—a proposal for uniform nomenclature. Nat. Rev. Immunol. *13*, 145–149.

Stergachis, A.B., Neph, S., Sandstrom, R., Haugen, E., Reynolds, A.P., Zhang, M., Byron, R., Canfield, T., Stelhing-Sun, S., Lee, K., et al. (2014). Conservation of *trans*-acting circuitry during mammalian regulatory evolution. Nature *515*, 365–370.

Stetson, D.B., Mohrs, M., Reinhardt, R.L., Baron, J.L., Wang, Z.E., Gapin, L., Kronenberg, M., and Locksley, R.M. (2003). Constitutive cytokine mRNAs mark natural killer (NK) and NK T cells poised for rapid effector function. J. Exp. Med. *198*, 1069–1076.

Tindemans, I., Serafini, N., Di Santo, J.P., and Hendriks, R.W. (2014). GATA-3 function in innate and adaptive immunity. Immunity *41*, 191–206.

Trapnell, C., Roberts, A., Goff, L., Pertea, G., Kim, D., Kelley, D.R., Pimentel, H., Salzberg, S.L., Rinn, J.L., and Pachter, L. (2012). Differential gene and transcript expression analysis of RNA-seq experiments with TopHat and Cufflinks. Nat. Protoc. *7*, 562–578.

Vahedi, G., Takahashi, H., Nakayamada, S., Sun, H.-W., Sartorelli, V., Kanno, Y., and O'Shea, J.J. (2012). STATs shape the active enhancer landscape of T cell populations. Cell *151*, 981–993.

Verykokakis, M., Zook, E.C., and Kee, B.L. (2014). ID'ing innate and innate-like lymphoid cells. Immunol. Rev. *261*, 177–197.

Visel, A., Blow, M.J., Li, Z., Zhang, T., Akiyama, J.A., Holt, A., Plajzer-Frick, I., Shoukry, M., Wright, C., Chen, F., et al. (2009). ChIP-seq accurately predicts tissue-specific activity of enhancers. Nature *457*, 854–858.

Wilson, C.B., Rowell, E., and Sekimata, M. (2009). Epigenetic control of T-helper-cell differentiation. Nat. Rev. Immunol. *9*, 91–105.

Xu, H., Luo, X., Qian, J., Pang, X., Song, J., Qian, G., Chen, J., and Chen, S. (2012). FastUniq: a fast de novo duplicates removal tool for paired short reads. PLoS ONE *7*, e52249.

Zang, C., Schones, D.E., Zeng, C., Cui, K., Zhao, K., and Peng, W. (2009). A clustering approach for identification of enriched domains from histone modification ChIP-Seq data. Bioinformatics *25*, 1952–1958.

Zhang, Y., Liu, T., Meyer, C.A., Eeckhoute, J., Johnson, D.S., Bernstein, B.E., Nusbaum, C., Myers, R.M., Brown, M., Li, W., and Liu, X.S. (2008). Model-based analysis of ChIP-seq (MACS). Genome Biol. *9*, R137.

Zhong, C., Cui, K., Wilhelm, C., Hu, G., Mao, K., Belkaid, Y., Zhao, K., and Zhu, J. (2016). Group 3 innate lymphoid cells continuously require the transcription factor GATA-3 after commitment. Nat. Immunol. *17*, 169–178.